

Thin Film Solar Cells

This chapter starts with a brief overview about the current state-of-the-art of photovoltaic devices based on CuInS_2 absorber layers. Then, the current voltage behavior of $\text{Cu}(\text{In}_{1-x}\text{Ga}_x)\text{S}_2/\text{CdS}/\text{ZnO}$ heterojunctions based on the absorber layers discussed in the previous chapter is described. The influence on the degree of alloying, i.e. the Ga-content x of the $\text{Cu}(\text{In}_{1-x}\text{Ga}_x)\text{S}_2$ phase, is investigated with respect to the attainable voltage under open circuit and standard illumination conditions. The found correlation between the Ga-content of the absorber layer and the open circuit voltage is discussed in the frame work of the grain boundary diffusion model introduced in the previous chapter.

4.1 Solar Cells Based on CuInS_2

First photovoltaic devices based on CuInS_2 have been reported by Kazmerski et al. [58] in 1977. Lewerenz et al. [142] achieved an energy conversion of 9.7 % with an electrochemical cell based on a CuInS_2 single crystal in 1986. An efficient thin film device followed in 1988 with an efficiency of 7.3 % by Michell et al. [143]. Thin film solar cells based on sequentially prepared CuInS_2 absorber layers have currently reached conversion efficiencies of 12.7% [10, 11]. This value is clearly below the current 18.8 % record efficiency of $\text{Cu}(\text{In}_{0.8}\text{Ga}_{0.2})\text{Se}_2$ based cells [3], but one has to note that such champion devices are achieved by means of sophisticated growth processes on a laboratory scale. Chalcopyrite devices obtained from more simple, technologically relevant preparation processes have so far reached efficiencies around 15%.

Nevertheless, from a theoretical point of view, the energy conversion efficiency of CuInS_2 based devices is still far below the calculated limit of approximately 30 % for an ideal solar cell with a band gap of 1.52 eV [12]. As can be seen in Table 4.1 this is mainly due to a moderate open circuit voltage V_{oc} . So far, this limitation was found to be inherent to the thin film material as various thin film growth techniques led to similar V_{oc} values in the range of 700 mV to 740 mV. Up to now several attempts have been reported in order to overcome this limitation, i.e.

- (a) absorber layer growth under Cu-poor conditions,
- (b) modifying the absorber/buffer interface, and

(c) alloying of the absorber layer by iso-valent and non iso-valent substitutions and/or by formation of solid solutions.

Each approach will be briefly outlined in the following.

Table 4.1: PV-parameters of an ideal solar cell with a band gap of 1.52 eV (taken from [12]) compared to values of the best so far achieved CuInS₂ thin film solar cell [11].

	ideal cell	CuInS ₂ thin film solar cell
j_{sc}	27.1 mA/cm ²	24.3* mA/cm ²
V_{oc}	1249 mV	729.4 mV
ff	90.1 %	71.7 %
η	30.5 %	12.7* %

* active area values, cell area = 0.511 cm²

(a) Cu-poor film growth In terms of photovoltaic energy conversion the most efficient CuInS₂ based thin film heterojunctions are currently achieved in a Cu-rich growth regime where a secondary Cu-S phase is present during thin film formation. The importance of this secondary phase with respect to the incorporation of sulfur has already been mentioned in Section 1.1.2. Furthermore, as was shown in this work, the presence of the binary phase greatly influence the cation ordering of the chalcopyrite (Section 3.3) and the cation interdiffusion in Cu(In_{1-x}Ga_x)S₂ layers of graded composition (Section 3.5.2). However, prior to the deposition of a transparent *n*-type layer onto the *p*-type chalcopyrite absorber the secondary Cu-S phase has to be removed by a cyanide etching step. It is not fully clear how far the KCN-etch influences and possibly degrades the electronic surface properties. However, for large scale production it may be preferable to avoid the etching step by stoichiometric or Cu-poor chalcopyrite layer growth which does not lead to secondary phase segregation. Unfortunately Cu-poor prepared CuInS₂ thin films generally suffer from low carrier densities which makes them unsuitable for heterojunction preparation (Section 1.1.2). Nevertheless, using coevaporation of the elements for absorber layer growth Scheer et al. [144] have achieved a 8.3 % efficient device. Carefully adjusted Na-doping has been used by Watanabe et.al [14] in order to grow device grade material without Cu-excess. They reported a conversion efficiency of 10.6 % recently.

(b) Buffer layer modifications Applying numerical device simulations Klenk [7] has pointed out the crucial role of the interplay between electronic properties (such as interface defect states) and band line up of the CuInS₂/window-layer interface for optimum diode behavior of the heterojunction (see Section 1.2.2). Modifying the buffer material and/or buffer deposition process might therefore be a way towards improving the properties of the junction allowing for higher conversion efficiencies. Indeed Braunger et al. [145] were able to substantially increase V_{oc} by adjusting the preparation conditions of the chemical bath for CdS-buffer deposition. Based on Braungers results the growth conditions of the

CdS layer used for devices reported here were modified in order to minimize the dark saturation current density of the heterojunction. However, no increase in V_{oc} beyond the (700–740) mV limit mentioned above could be achieved by buffer layer modifications. The same set of growth parameters, which is considered to be the current optimum for a $\text{CuInS}_2/\text{CdS}$ interface, was used throughout this work for buffer layer deposition.

Another approach towards improved interface properties is the replacement of the commonly used CdS by an alternative material. Such a modification is motivated in addition by environmental concerns regarding the toxicity of Cd. Good results have so far been achieved using buffer layers based on $(\text{In,Zn})_x(\text{OH,S})_y$ compounds [146–148]. The best Cd-free CuInS_2 -based solar cell, reported up to now, achieved an active area efficiency of 11.4% [146]. However, up to now no significant technical “break through” has been achieved by replacing the “classical” CBD-CdS buffer layer with alternative materials.

(c) Absorber alloying/Solid solutions The incorporation of isovalent or non-isovalent substitution into the absorber has been proven to be a very successful way towards chalcopyrite thin films suitable for highly efficient photovoltaic devices. It is one of the advantages of the ternary I-III-VI₂ compounds that characteristic material properties, such as lattice constants and band gaps can be controlled to some extent, by adjusting the concentration of iso-valent substitutions resulting in quaternary (e.g. $\text{Cu}(\text{In,Ga})\text{Se}_2$) or even pentenary compounds (e.g. $\text{Cu}(\text{In,Ga})(\text{S,Se})_2$) (Section 1.1.1).

Furthermore the finding that controlled incorporation of CuInSe_2 with sodium leads to more efficient devices, was another major prerequisite for processing high efficiency photovoltaic devices. The effect of Na is likely to be an indirect one, since, according to Braunger [37], Na (and also Ga) has an enhanced affinity towards Se, thus it influences the adsorption of selenium during thin film formation and reduces the density of selenium vacancies, which act as compensating donors in the film.

Current thin film record devices are achieved by substituting In partially by Ga in a CuInSe_2 based absorber layer. Thereby the band gap is shifted to a value that better matches the solar spectrum. The effects of Ga onto the growth process and the structural properties of chalcopyrite thin films have already been discussed in Chapter 3 of this work.

In CuInS_2 -based thin film solar cells preliminary results on the effects of gallium incorporation have been published only recently. Villora [107] and Hengel et al. [149] reported on slightly improved open circuit voltages due to gallium addition. Watanabe et al. [14] achieved an open circuit voltage of 780 mV by incorporation of Ga into the CuInS_2 absorber layer. Similarly high V_{oc} values for $\text{Cu}(\text{In,Ga})\text{S}_2$ based absorber layers could be achieved by Dhare et al. [150]. Furthermore gallium was found to increase absorber layer adhesion to the back contact [43].

As the type of conductivity and the carrier density in Cu-chalcopyrites is determined by intrinsic defects and a high level of compensation deliberately influencing the effective acceptor or donor concentration by incorporation of an isovalent or non-isovalent species is in

general a complex issue [21]. This is partly due to Fermi level dependent defect formation which is characteristic for this type of compound semiconductors [151, 152]. A self compensation mechanism in these materials restricts the doping of the material to certain limits (see e.g. [153]), which occurs because shifting the Fermi-level beyond some critical value by introducing additional dopants, leads to the formation of lattice defects compensating the higher dopant concentration.

Nevertheless, there are a number of reports in literature about reproducible changes in the effective carrier concentration due to the incorporation of an impurity metal. Although the underlying changes in the defect chemistry of the chalcopyrite are still not fully identified, correlations between the electronic properties of the material and the impurity have been given. It was shown by Braunger et al. [145] and Luck et al. [154] that the incorporation of small amounts of Zn into the CuInS₂ absorber turned out to be a way towards higher V_{oc} values of CuInS₂/CdS/ZnO solar cells. Unfortunately, both authors report on severe degradation of other photovoltaic parameters, especially fill factor with Zn-incorporation. Another example is the addition of Ag in sequentially prepared CuInS₂ thin films, which was shown to reduce the lateral film conductivity [155]. Although, in CuInS₂ thin films grown under In-rich conditions, a dependence of film conductivity on the Na and O concentration was found [156], no correlation between device performance of Cu-rich processed CuInS₂ absorber layers and the amount of Na (realized by using different glass substrates) could be observed [157]. As discussed in Section 1.1.2 this is due to the presence of the copper sulfide phase which assists the incorporation of sulfur during film growth. The independence of the CuInS₂ film properties on the Na-content of the layer marks one of the advantages of CuInS₂ thin film growth under Cu-rich conditions in a potential large scale production environment in comparison to CuInSe₂ based devices where a careful tuning of the Na-content is required.

4.2 Cu(In_{1-x}Ga_x)S₂/CdS/ZnO Heterojunctions

As mentioned above it had already been shown that incorporation of moderate amounts of Ga into a CuInS₂ absorber layer is a remedy which can be used to increase the open circuit voltage. These findings were one of the major motivations for a more detailed investigation of the properties of Cu(In_{1-x}Ga_x)S₂ ($0.0 < x < 0.3$) thin films as presented in this work. This section will demonstrate the influence of Ga-alloying onto the photovoltaic properties of a Cu(In_{1-x}Ga_x)S₂/CdS/ZnO junction.

As was shown in chapter 3 the structural quality of the Cu(In_{1-x}Ga_x)S₂ layers as well as the depth profile of the Ga-concentration can be influenced by precursor composition, temperature and time of the reactive annealing step. Furthermore, it was shown that the Cu(In_{1-x}Ga_x)S₂ layers generally crystallize in a two layer structure. The top layer consists of a phase close to CuInS₂ whereas the composition of the back layer phase is close to CuGaS₂. The Ga-concentration in top and back layer is $x < 0.15$ and $x > 0.75$

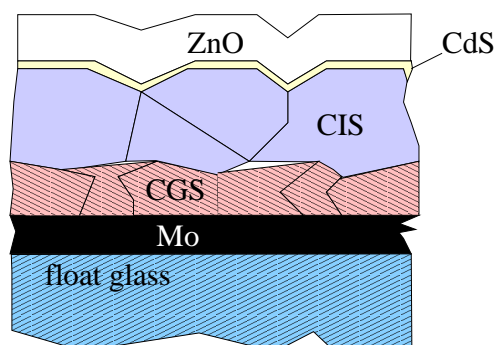


Figure 4.1: Structure of $\text{Cu}(\text{In}_{1-x}\text{Ga}_x)\text{S}_2/\text{CdS}/\text{ZnO}$ heterojunction (not to scale).

respectively. In order to investigate how effects of variations in the discussed structural properties (cation ordering, Ga depth profile) correlate with the electrical behavior of a heterojunction differently prepared absorber layers have been completed by a CdS/ZnO window layer. Some details on the solar cell preparation process can be found in Section 2.1 and also in [65, 158]. The schematic structure of such a heterojunction is depicted in Figure 4.1. The heterojunctions were then analyzed by j - V curve measurements (with and without standard AM 1.5 illumination [159]) and by spectral photo response measurements (Section 1.2.3). In the following samples are denoted according to their respective absorber layer growth conditions.

j - V characteristics When describing the photovoltaic properties of a solar cell the current voltage characteristics (j - V curve) is characterized by four parameters: the conversion efficiency η , the short circuit current density j_{sc} , the open circuit voltage V_{oc} , and the fill factor ff (see Section 1.2). Figure 4.2 compares the j - V curve of an efficient $\text{CuInS}_2/\text{CdS}/\text{ZnO}$ heterojunction with a junction based on a $\text{Cu}(\text{In}_{1-x}\text{Ga}_x)\text{S}_2$ absorber prepared in the course of this work. The addition of gallium (precursor: $[\text{Ga}]/([\text{In}]+[\text{Ga}])=0.3$) has led to an increase in open circuit voltage by more than 70 mV. In contrast to earlier results on V_{oc} improvements in CuInS_2 based solar cells (Section 4.1) the V_{oc} gain is not accompanied by any degradation of the rectifying properties of the junction, i.e. no degradation in fill factor was observed. As a result the $\text{Cu}(\text{In}_{1-x}\text{Ga}_x)\text{S}_2/\text{CdS}/\text{ZnO}$ heterojunction energy conversion efficiency increases by 5%. The observed increase in open circuit voltage depends strongly on the Ga-content of the Cu-In-Ga precursor and on growth conditions during reactive annealing. Figure 4.3 shows a clear correlation between V_{oc} and the $[\text{Ga}]/([\text{In}]+[\text{Ga}])$ ratio of the precursors used for absorber preparation. An overview of the device parameters of several solar cells processed from $\text{Cu}(\text{In}_{1-x}\text{Ga}_x)\text{S}_2$ absorber layers sulfurized in elemental sulfur or in $\text{H}_2\text{S}/\text{Ar}$ is given in Table 4.2.

A systematic variation of those parameters, that were found to influence the Ga-depth profile (see Chapter 3), such as the precursor Ga-content, the substrate temperature during the reactive annealing step and the duration of the annealing step, revealed the following correlations between the thin film growth conditions of the absorber layer and the PV-parameters of the resulting devices:

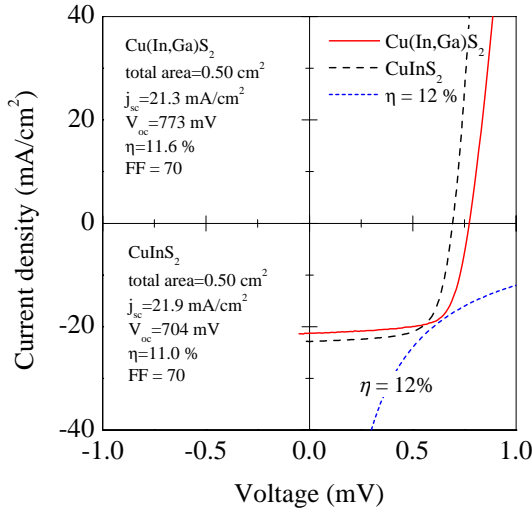


Figure 4.2: j - V characteristics under illumination (simulated AM 1.5 conditions) of a standard $\text{CuInS}_2/\text{CdS}/\text{ZnO}$ heterojunction and a $\text{Cu}(\text{In}_{1-x}\text{Ga}_x)\text{S}_2/\text{CdS}/\text{ZnO}$ heterojunction.

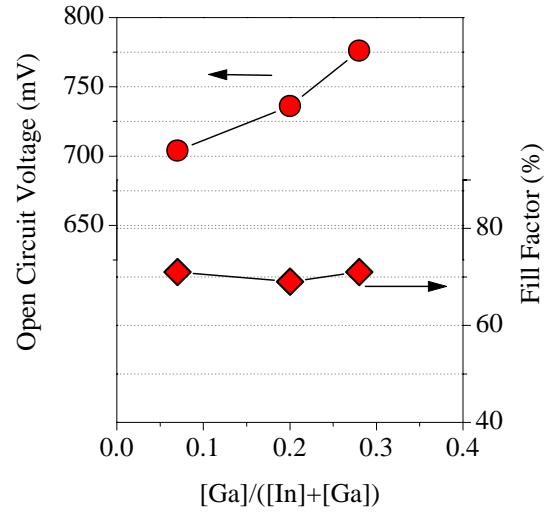


Figure 4.3: Open circuit voltage and fill factor of $\text{Cu}(\text{In}_{1-x}\text{Ga}_x)\text{S}_2/\text{CdS}/\text{ZnO}$ heterojunctions having different precursor $[\text{Ga}]/([\text{In}] + [\text{Ga}])$ ratios. All absorbers have been processed in sulfur vapor at 550°C for 30 min.

Table 4.2: PV-parameters of several $\text{Cu}(\text{In}_{1-x}\text{Ga}_x)\text{S}_2$ based solar cells under standard illumination conditions AM 1.5 (incident total light intensity $P_i = 100 \text{ mW}/\text{cm}^2$).

sample	$[\text{Ga}]/([\text{In} + \text{Ga}]^*$	T_{sulf} ($^\circ\text{C}$)	t_{sulf} (min)	η (%)	V_{oc} (mV)	ff (%)	j_{sc} (mA/cm^2)
elemental S							
Ga-free	0	550	30	11.0	704	71	21.9
S-550-20	0.2	550	30	10.4	736	69	10.4
S-550-30	0.3	550	30	10.0	776	71	18.1
S-600-15	0.3	600	15	10.9	829	70	18.7
S-600-30	0.3	600	30	11.6	811	71	20.1
Ar/ H_2S							
Ga-free	0	525	5	10.1	701	70	20.5
H_2S -475-10	0.3	475	10	9.7	751	65	19.7
H_2S -500-10	0.3	500	10	11.6	772	70	21.3
H_2S -525-15	0.3	525	15	11.3	777	73	20.0
H_2S -550-15	0.3	550	15	9.0	824	60	17.7

* values refer to Ga-concentration of precursor layers

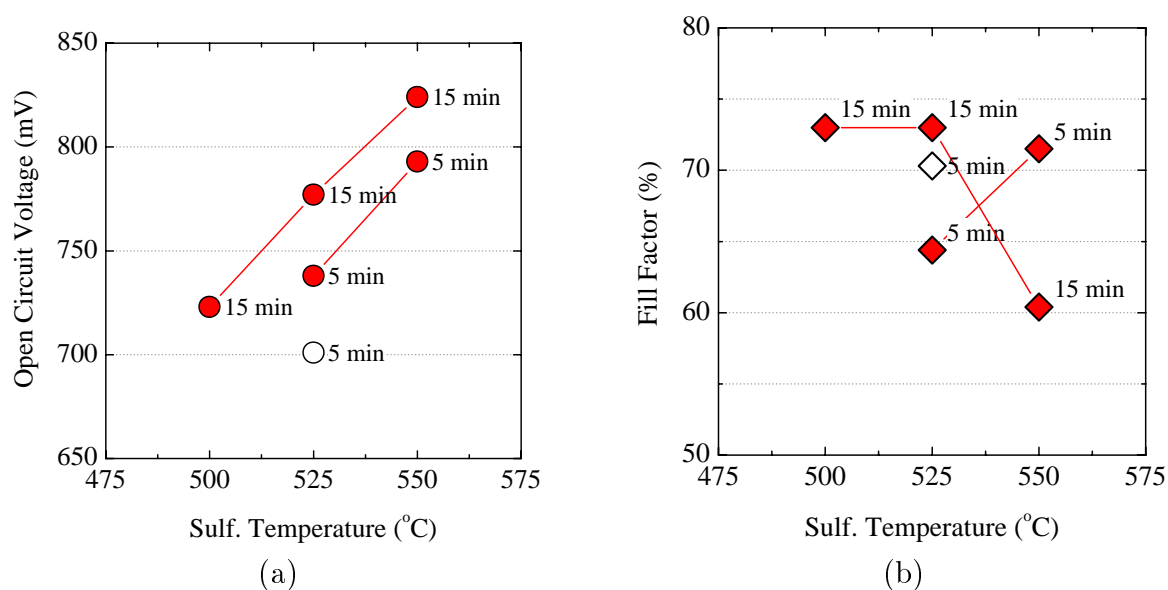


Figure 4.4: (a) Open circuit voltage and (b) fill factor of gallium containing devices as a function of sulfurization time and temperature (labels denote sulfurization time). The open symbol refers to a Ga-free reference sample.

1. In the range of moderate precursor Ga-concentrations ($[\text{Ga}]/([\text{In}] + [\text{Ga}]) < 0.3$) the open circuit voltage V_{oc} of a $\text{Cu}(\text{In}_{1-x}\text{Ga}_x)\text{S}_2$ based solar cell depends directly on sulfurization temperature. Increasing T_{sulf}^* to values just below the melting point of the glass substrate leads to V_{oc} values well above 830 mV, which is more than 100 mV higher than the Ga-free reference and more than 50 mV higher than the V_{oc} -values of $\text{Cu}(\text{In}_{1-x}\text{Ga}_x)\text{S}_2$ -based reported so far. Figure 4.4 shows the clear correlation between V_{oc} and the sulfurization conditions in a series of samples in which all absorber layers were processed from identical precursors, but sulfurization time and temperature were varied. As will be shown below the effect correlates with the Ga-concentration of the $\text{Cu}(\text{In}_{1-x}\text{Ga}_x)\text{S}_2$ top phase, which increases in a similar way with increasing temperature during film growth (Section 3.5.2).
2. Increasing the precursor $[\text{Ga}]/([\text{In}] + [\text{Ga}])$ ratio up to 0.3 leads to an open circuit voltages increase of 70 mV without any losses in fill factor or short circuit current. This is in clear contrast to earlier works where a substantial increase in open circuit voltage was always accompanied by a substantial loss in fill factor [145, 154]. The presented capability of Ga-alloying to increase the open circuit voltage of a CuInS_2 -based solar cell without degrading other device properties presents perhaps the most salient result of this work. There seems to be an optimum in the absorber Ga-content, as at higher Ga-concentrations the increase in V_{oc} tends to saturate and the fill factor starts to drop.
3. For moderate precursor $[\text{Ga}]/[\text{In} + \text{Ga}]$ ratios (< 0.3) no dependence of the fill factor on sulfurization temperature could be observed.

*Please note, that all absolute temperature values in figures as well as in the text are given as read at the meter. Systematic errors, found to be as high as 50 K, differ between different processing machines.

These trends have been proven to be very reproducible, regardless whether elemental sulfur or $\text{H}_2\text{S}/\text{Ar}$ was used for sulfurization. There is some scatter in the PV-parameters between nominally identical samples from different precursor batches which are probably due to random variations of the film thickness of the individual precursor layers. However, there is a very systematic dependence on sulfurization temperature and time when identical precursors were used (Figure 4.4).

Spectral Response It was shown in Section 3.5 that the degree of Ga-alloying of the top phase of the layer is determined by a thermally activated interdiffusion process. From the j - V data listed in Table 4.2 it becomes evident that increasing alloying of the $\text{Cu}(\text{In}_{1-x}\text{Ga}_x)\text{S}_2$ top phase of the absorber layer at higher sulfurization temperatures leads to higher open circuit voltages. Since the band gap of the $\text{Cu}(\text{In}_{1-x}\text{Ga}_x)\text{S}_2$ alloy system increases almost linearly with composition x (Section 1.1.3) and a larger band gap at the absorber/CdS interface can, in principle, lead to an increase in open circuit voltage (Section 1.2.2) quantum efficiency measurements have been employed in order to get a quantitative measure of the absorber band gap. The slightly lower short circuit current densities j_{sc} for samples with V_{oc} values exceeding 770 mV are a first indication for a Ga-induced band gap widening in the absorber layer.

In order to quantify the Ga-induced bandgap shift the first derivative of the EQE spectra around the absorption edge has been evaluated (Section 1.2.3). In the following an effective band gap value $E_{g,\text{eff}}$ will be introduced which refers to the maximum in $dEQE/dh\nu$ around the absorption edge, and which will be used as an estimate for the band gap value of the absorber (Section 1.2.3).

In Figure 4.5 the normalized quantum efficiencies and the first derivative are plotted. The same set of samples already discussed in Table 4.2 is considered here. For Ga-free devices the first derivative shows one maximum (denoted $E_{g,\text{eff}}^{(2)}$ in the Figure 4.5) at around 825 nm, which corresponds to $E_{g,\text{eff}} = 1.51$ eV. The derivative of the EQE spectra of Ga-free devices exhibit an additional shoulder at the longer wavelength side. This tail below $EQE = 0.4$ disappears in case of Ga-containing absorber layers, suggesting reduced sub-band gap absorption in Ga-containing absorber layers. The addition of Ga also leads to a shift of the absorption edge towards shorter wavelength. This verifies the assignment of the already observed shift in lattice constant (Section 3.5) to the incorporation of Ga into the top phase. Up to 100 meV shift in the position of the absorption edge can be observed for samples sulfurized at temperatures between 475 °C and 550 °C in $\text{H}_2\text{S}/\text{Ar}$. However, the determination of an effective band gap value in Ga-containing devices is not as straightforward as in the Ga-free case. With increasing precursor $[\text{Ga}]/([\text{In}] + [\text{Ga}])$ ratio a second peak evolves in the first derivative of the EQE (denoted $E_{g,\text{eff}}^{(2)}$). The peak can not be explained by a second direct transition due to a Ga-induced lifting of the degeneracy of the valence band (Section 1.1.3). Although Ga-incorporation influences the valence band splitting which is due to the tetrahedral field, at the Ga-concentrations discussed

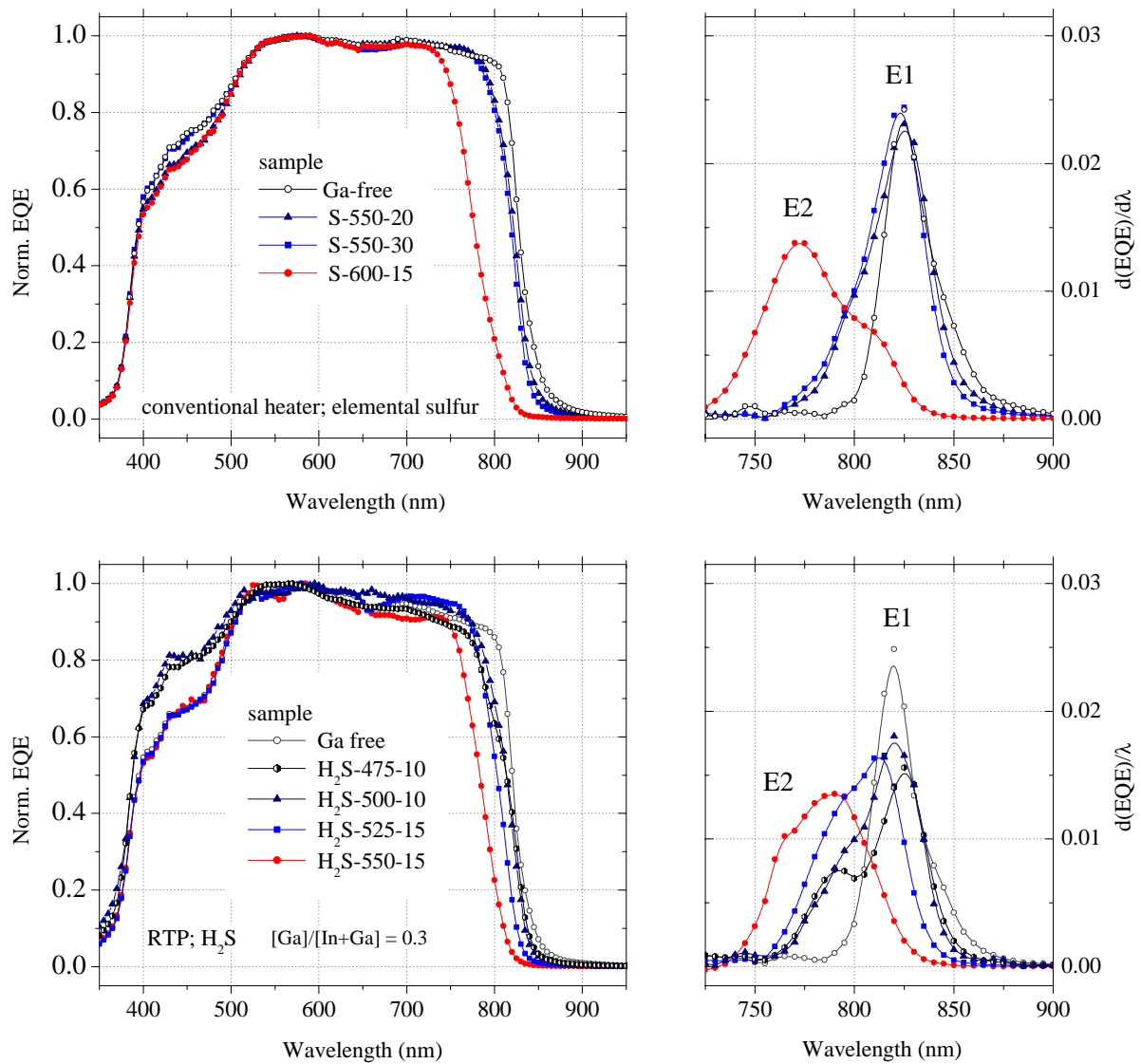


Figure 4.5: Normalized external quantum efficiency of solar cells. *upper row*: sulfurized in elemental sulfur, *lower row*: sulfurized in H_2S . Sample details can be found in Table 4.2.

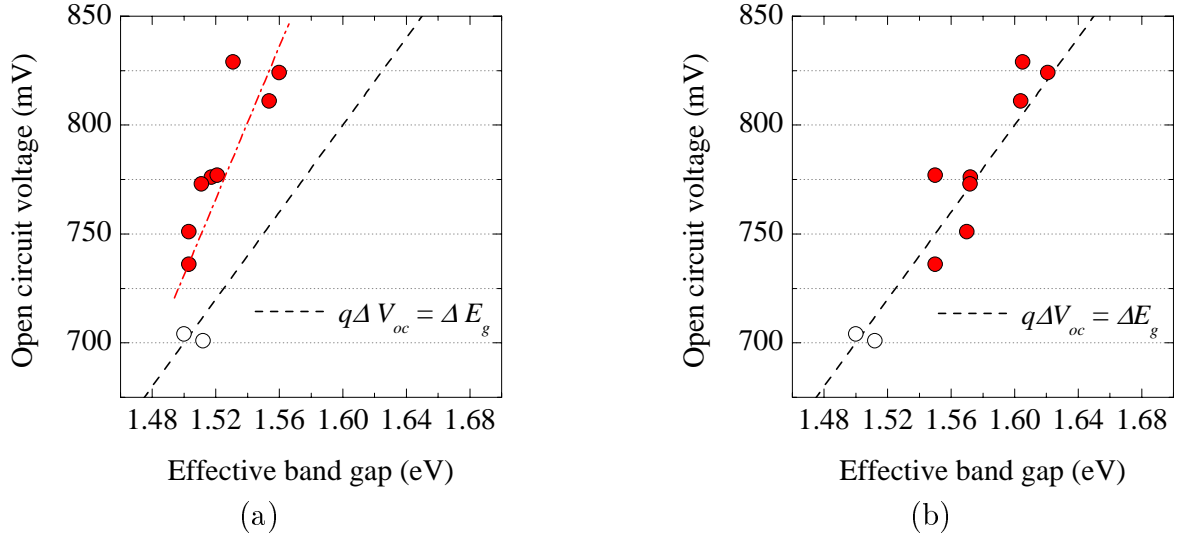


Figure 4.6: Open circuit voltage of $\text{Cu}(\text{In}_{1-x}\text{Ga}_x)\text{S}_2/\text{CdS}/\text{ZnO}$ solar cells versus effective absorber band gap as derived from (a) peak E1 and (b) peak E2 of the first derivative $dEQE/dh\nu$ of the external quantum efficiency around the absorption edge. The dashed line serves as a reference line that assumes a 1:1 relation between $\Delta E_{g,\text{eff}}$ and ΔqV_{oc} .

here ($[\text{Ga}]/([\text{In}] + [\text{Ga}]) < 0.3$), the effect accounts for less than 30 meV. The separation between $E_{g,\text{eff}}^{(1)}$ and $E_{g,\text{eff}}^{(2)}$ is more than 60 meV. As can be seen in Figure 4.5 the values of $E_{g,\text{eff}}^{(1)}$ and $E_{g,\text{eff}}^{(2)}$ are a function of sulfurization temperature, however they are not greatly affected by variation in the precursor $[\text{Ga}]/([\text{In}] + [\text{Ga}])$ ratio from 0 to 0.3. This agrees with the behavior found for the incorporation of Ga in Section 3.5. On the basis of lattice constants of the top phase determined by XRD (Figure 3.27), significant Ga-incorporation was only observed for samples sulfurized at elevated substrate temperatures, i.e. there was no correlation to the precursor Ga-content.

In order to estimate how far the gain in V_{oc} is due to a shift in E_g to higher energies the V_{oc} values have been plotted versus the $E_{g,\text{eff}}^{(1)}$ and $E_{g,\text{eff}}^{(2)}$ values deduced from $dEQE/dh\nu$. As can be seen in Figure 4.6 (a) the gain in V_{oc} is clearly higher than the shift in the band gap value $E_{g,\text{eff}}^{(1)}$. In particular for small shifts in the band gap value $E_{g,\text{eff}}^{(1)}$ the V_{oc} increases by 50 meV without any significant shift in band gap.

The situation is different if the open circuit is related to the $E_{g,\text{eff}}^{(2)}$ value. Here the plot (Figure 4.6 clearly proposes a linear relation between the gain in V_{oc} and the shift in absorber band gap. Thus, whereas the $E_{g,\text{eff}}^{(1)}$ band gap value seems to be related to the Ga-alloying of the top phase of the absorber layer as determined by XRD, the $E_{g,\text{eff}}^{(2)}$ value shows a clear correlation to the open circuit voltage V_{oc} of the respective device. Several effects which could cause an increase in V_{oc} are discussed below.

4.2.1 The Ga-Induced Gain in V_{oc}

The experimental data presented in the previous section clearly shows that the degree of interdiffusion, i. e. the Ga content in the active region of the cell influences the absorber band gap as well as the open circuit voltage. As already discussed in Section 1.2.2, the correlation of the gain in open circuit voltage ΔV_{oc} for a given increase in band gap ΔE_g depends on the dominating recombination mechanism. Two cases have been distinguished: 1.- recombination in the space charge region which yields a simple $\Delta V_{oc} \approx \Delta E_g$ relationship, and, 2.- recombination at the interface where a cliff in the conduction band causes a reduced barrier and where the open circuit gain depends on whether the band gap widening influences mainly the conduction or valence band, respectively.

The former case is well known from the Cu(In_{1-x}Ga_x)Se₂-based solar cells with moderate Ga-content ($x < 0.3$). Analyzing the current-voltage characteristics of these cells reveals recombination in the space charge region as the dominating recombination mechanism and there is a clear correlation between the bulk defect density as determined from admittance spectroscopy and the recombination losses. Experimental data also confirm the correlation between band gap and open circuit voltage [4, 47, 50].

Figure 4.6 (b) may suggest a similarly simple model for the open circuit voltage of the Cu(In_{1-x}Ga_x)S₂-solar cells of this work. In addition, Kneisel et.al. [160] report on an empirical correlation between a deep absorber bulk defect and recombination losses in a certain type of CuInS₂/CdS/ZnO solar cells. However, Hengel [45] and Reiss [161] have shown that neither the activation energy of the saturation current of the illuminated cell nor the extrapolation of the open circuit voltage to 0 K are consistent with the assumption of recombination in the space charge region. Also, admittance spectroscopy performed on the cells prepared here with varied Ga-content were not conclusive. It is therefore necessary to derive a model based on the second case given above.

Photoelectron spectroscopy indeed suggests that there is a cliff at the CuInS₂/CdS interface. Experimental values for the valence band offset ΔE_{VBM} range from 0.6 eV, measured at single crystals [162], to 1.2–1.5 eV for thin film substrates [163, 164]. There is no experimental data on the CuGaS₂/CdS band line-up, so in order to predict the behavior of a Cu(In_{1-x}Ga_x)S₂/CdS interface one is bound to theoretical considerations. Scheer [165] has estimated the band line-up for several Cu-chalcopyrite/II-VI heterointerfaces using a simple linear model, which assumes that the charge neutrality levels are aligned at the interface and which considers strain effects and differences in the electronegativity of the elements on either side of the interface. In Table 4.3 some of his results are listed. According to Scheer's predictions, which are in good agreement with experimental results in the case of the Cu(In_{1-x}Ga_x)Se₂/CdS system, gallium in Cu(In_{1-x}Ga_x)S₂ should lead to a shift not only of the valence band but of the conduction band too. Then, a widened absorber band gap would lead to a higher barrier at the interface. The resulting band line up at a Cu(In_{0.8}Ga_{0.2})S₂/CdS interface is plotted in Figure 4.7. Based on these estimations of the band line-up the systematic increase of the open circuit voltage with increasing shift of the absorption edge can be explained also for the interface limited devices of this work.

However, even if the total gap shift would be accommodated in the valence band, the observed gain in open circuit voltage is still higher than expected. It has been suggested that Ga incorporation will, in addition to the band gap widening, also lead to a decrease of the interface density of states [45] which would explain this observation. Taking into account the complex defect chemistry of the absorber material and the ex-situ preparation of the heterointerface, the very systematic trend observed in this work for a large number of differently prepared devices makes it unlikely that the density of states plays such a significant role. An alternative model consistent with the experimental data of this work and based on the diffusion of Ga along grain boundaries to the absorber surface is proposed in the following.

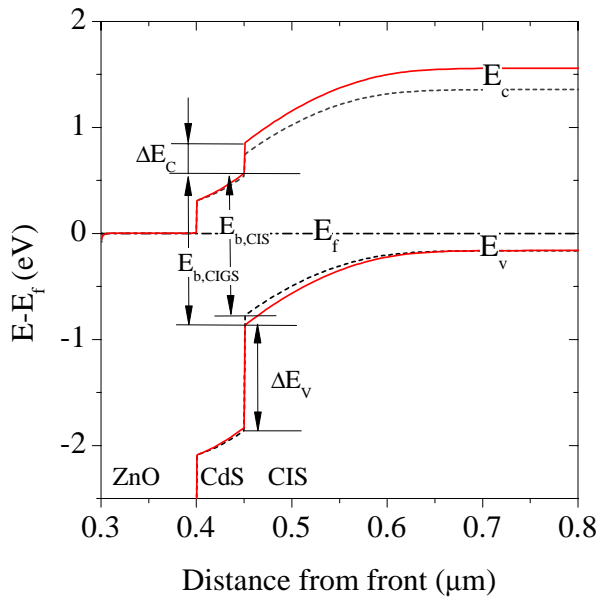


Figure 4.7: Valence band-lineup of a $\text{CuInS}_2/\text{CdS}$ (dashed line) and a $\text{Cu}(\text{Ga}_{0.2}\text{In}_{0.8})\text{S}_2/\text{CdS}$ (solid line) heterointerface. The valence band offset of the $\text{Cu}(\text{Ga}_{0.2}\text{In}_{0.8})\text{S}_2/\text{CdS}$ is based on values given in Table 4.3 assuming a linear dependence of ΔE_{VBM} on composition x . E_b refers to the barrier height for carriers at the CIGS/CdS interface assuming interface recombination as the dominant recombination mechanism.

In view of the Ga-In interdiffusion model introduced in Chapter 3 it has to be concluded that the observed V_{oc} gain is rather due to a band gap widening effect at the absorber

Table 4.3: Predicted values for valence band-lineup of $\text{CuInSe}_2/\text{CdS}$, $\text{CuGaSe}_2/\text{CdS}$, $\text{CuInS}_2/\text{CdS}$ and $\text{CuGaS}_2/\text{CdS}$ interfaces (from Ref. [165]).

	$\text{CuInSe}_2/\text{CdS}$	$\text{CuGaSe}_2/\text{CdS}$	$\text{CuInS}_2/\text{CdS}$	$\text{CuGaS}_2/\text{CdS}$
ΔE_{VBM} (eV) from experiment				
single x-tals	0.8–0.9		0.6	
thin films	0.92–1.0		1.2–1.5	
ΔE_{VBM} (eV) as predicted by virtual gap states model				
	1.03	1.1	0.93	0.35
$\Delta E_{VBM}^{CIS} - \Delta E_{VBM}^{CGS}$ (eV)		-0.07		0.58

surface. It was shown in Section 3.5.2 that the Ga-rich Cu(In_{1-x}Ga_x)S₂ phase close to the back contact acts as a diffusant reservoir for diffusion of Ga into the top phase. This interdiffusion process could well be described by assuming a grain boundary diffusion model (Section 3.5.3). Since the secondary copper sulfide phase plays a crucial role as a high diffusivity path way in this diffusion process (Figure 3.31) Ga diffusion will not only proceed from the CuGaS₂ phase at the back and out of grain boundaries, as was considered in the diffusion model, but also out of the copper-sulfide phase which covers the absorber layer surface. Hence, the surface can be envisioned as an additional “grain boundary” which also contributes to the diffusion process. As a result the Ga-concentration close to the layer surface will be higher than in the bulk of the grain. In order to estimate the diffusion of Ga out of grain boundaries in the near surface region Ga iso-concentration contours have been calculated based on the grain boundary diffusion model of Gillmer and Farrell (Appendix A.2) which was already employed in Section 3.5.3. Figure 4.8 shows the Ga-concentration in a columnar grain of 1 μm width which is assumed to be embedded in a CuInS₂ layer of 2 μm thickness. The CuGaS₂ phase, the diffusant reservoir, is located along the *y*-axis. Figure 4.8 (a) plots the iso-concentration contours of the entire grain whereas subfigure (b) and (c) show sections of the Ga-concentration along the *z* = 2 μm-axis (surface) and along the *y* = 0 μm-axis (depth profile along middle of grain). Three different bulk diffusion coefficients are considered in the figure. Based on the results of Table 3.7 in Section 3.5.3 the values refer to chemical diffusion of Ga into CuInS₂ in the temperature range of 500 °C to 600 °C. The transition of a concentration profile dominated by grain boundary diffusion at $D = 5 \times 10^{-14} \text{ cm}^2\text{s}^{-1}$ ($D/\delta D_b = 2 \times 10^{-3}$) to a profile dominated by bulk diffusion at $D = 5 \times 10^{-13} \text{ cm}^2\text{s}^{-1}$ ($D/\delta D_b = 2 \times 10^{-2}$) can clearly be seen. It becomes evident from the simulated Ga-concentrations at *z* = 2 μm that close to the surface the Ga-concentration varies between ≈ 0.2 at the edge of the grain and zero in the bulk of the grain across a distance of approximately 200 nm. Assuming a similar profile for Ga-diffusion from the layer surface the resulting widened band gap in the near surface region will cause an increase in open circuit voltage, whereas the photocurrent collection which is determined by the bulk value of the band gap remains unaffected. In this terms the appearance of two effective band gap values for Ga-containing absorber layers can also be explained. Whereas $E_{g,\text{eff}}^{(1)}$ refers to the band gap in the bulk and, hence is not correlated to the open circuit voltage of the solar cell, $E_{g,\text{eff}}^{(2)}$ describes the band gap in the near surface region where V_{oc} and $E_{g,\text{eff}}^{(2)}$ are clearly correlated (Figure 4.6). Furthermore, this explains the correlation of the $E_{g,\text{eff}}^{(1)}$ values to the lattice constant values as determined by XRD, since both values refer to the bulk concentration of the CuInS₂ layer.

The assumed band gap gradient in the near surface region is furthermore confirmed by the EQE-spectra of Ga-containing cells, which show an reduced overall slope around the absorption edge (Figure 4.5). Simulated EQE-data based on a numerical evaluation of Equation (1.9), using the assumptions as stated in Section 1.2.3, and accounting for a depth gradient of the absorber band gap, clearly resemble the reduced slope of the EQE spectra. Figure 4.9 shows the assumed depth profile of the band gap in a Ga-free and in a Ga-containing absorber layer. The widening of the band gap in the near surface region, due

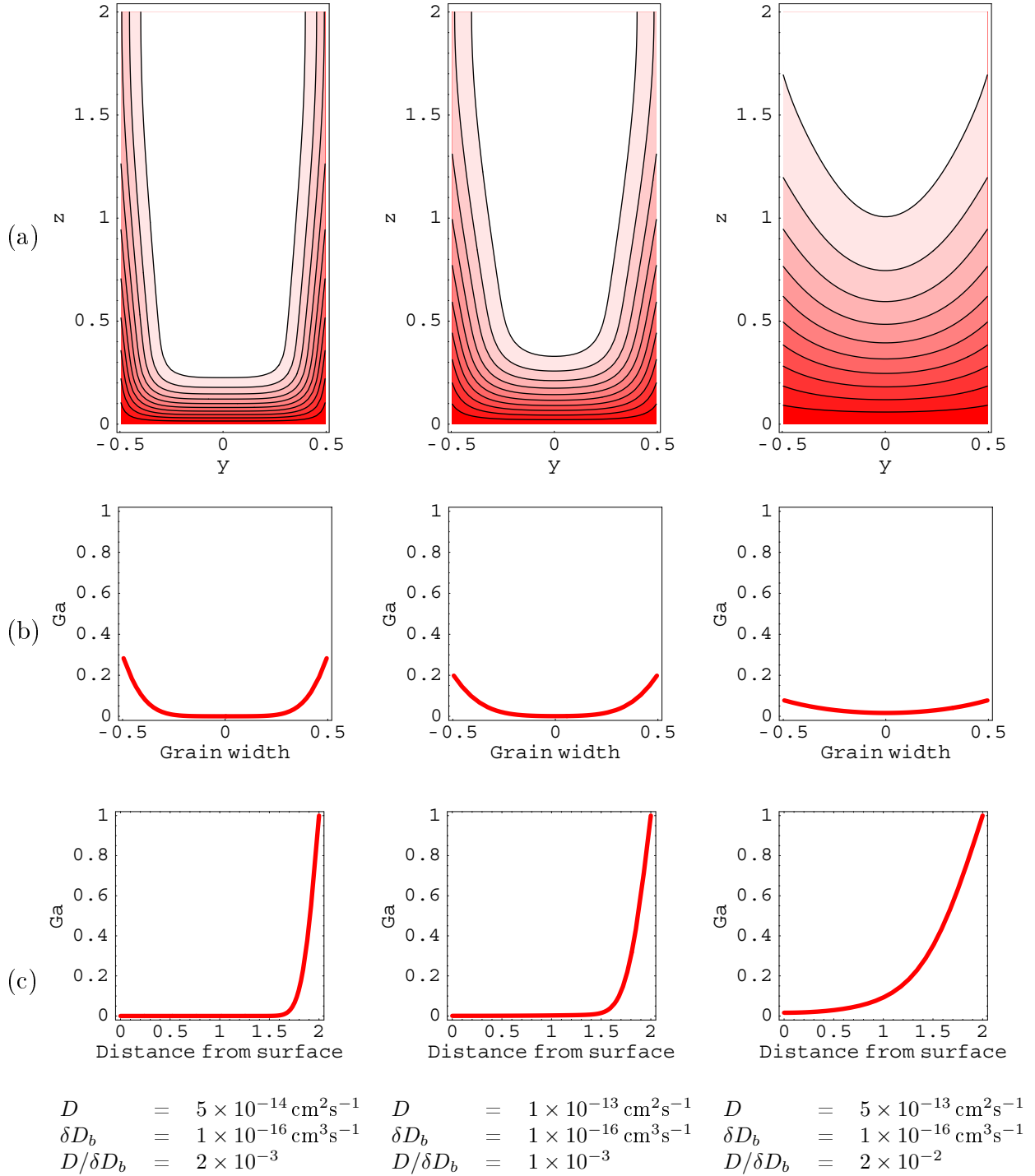


Figure 4.8: (a) Iso-concentration contours of $[Ga]/([In] + [Ga])$ ratio for a $CuInS_2$ grain for different bulk diffusion coefficients (film geometry acc. to Figure A.5); D = bulk diffusion coefficient, D_b = grain boundary diffusion coefficient, δ = width of grain boundary, (Iso-contour spacing $\Delta[Ga]/([In] + [Ga]) = 0.1$); (b) Corresponding $[Ga]/([In] + [Ga])$ ratio along $z = 2 \mu m$; (c) Corresponding $[Ga]/([In] + [Ga])$ ratio along $y = 0 \mu m$; (scaling of all axis $1 \mu m$, expect y -axis in (b) and (c)).

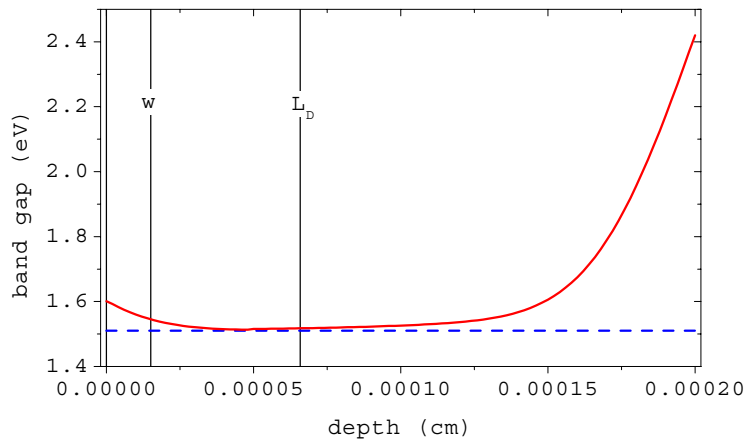


Figure 4.9: Modeled depth profile of band gap for simulation of EQE spectra of a Ga-free (dashed line) and a Ga-containing (solid line) solar cell. w denotes the width of the space charge region; L_D the diffusion length for electrons (x-axis scaling = 1 nm).

to the diffusion of Ga, leads to reduced carrier generation at photon wavelength just below the absorption edge (Figure 4.10). The resulting reduced result slope of the absorption edge in the EQE spectra can clearly be seen in both, the simulated data as well as in measured EQE spectra at $\text{Cu}(\text{In}_{1-x}\text{Ga}_x)\text{S}_2$ -based solar cells (Figure 4.11).

In conclusion solar cell devices based on $\text{Cu}(\text{In}_{1-x}\text{Ga}_x)\text{S}_2$ -thin films show an substantial increase in open circuit voltage under standard illumination conditions. In contrast to earlier attempts to increase the open circuit voltage of CuInS_2 -based devices the incorporation of moderate amounts of Ga into the active region of the cell does not degrade the characteristic photovoltaic parameters of the device especially the fill factor is sustained. The observed gain in V_{oc} with increasing Ga-concentration could be related to a theoretically predicted shift of the energetic position of the absorber valence band with Ga-alloying. However, it was also shown that the observed gain in V_{oc} can be solely explained by such a band gap widening effect, only if a graded band gap in the near interface region, caused by indiffusion of Ga from the surface, is assumed.

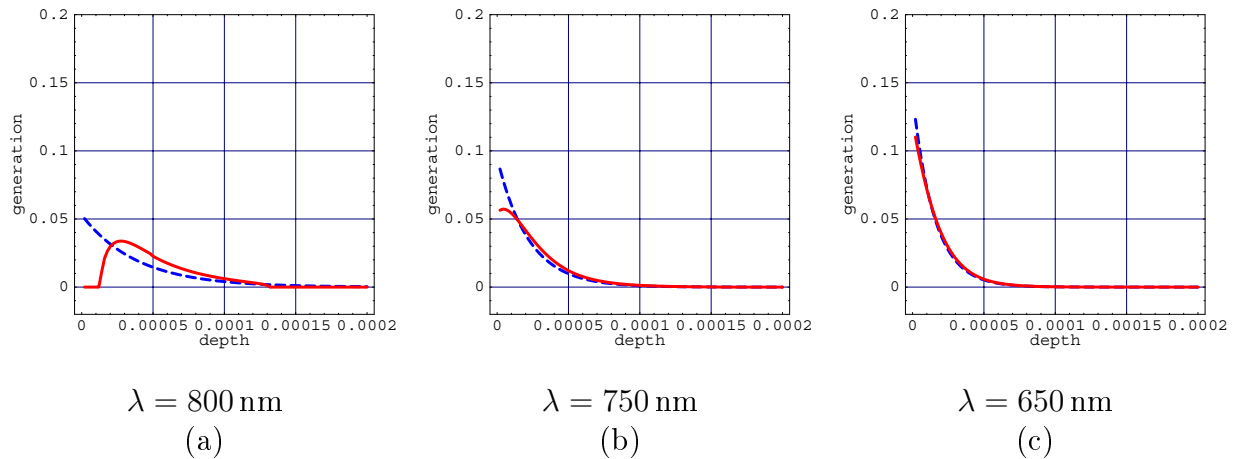


Figure 4.10: Calculated carrier generation profile $G(x) \propto \frac{dn(x)}{dx}$ ($n(x)$ = incident photon flux) for monochromatic illumination of different photon wavelength for a Ga-free (dashed line) and a Ga-containing (solid line) absorber layer (x-axis scaling = 1 cm).

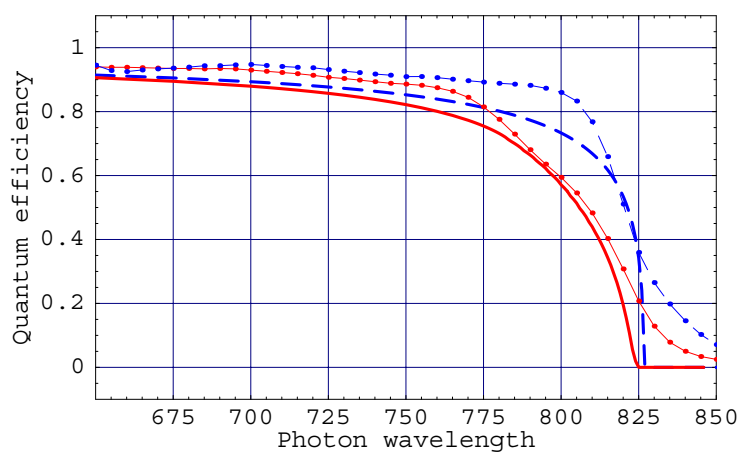


Figure 4.11: Modeled (lines) and experimental (symbol + lines) EQE-spectra of a Ga-free (dashed line) and a Ga-containing (solid line) solar cell (x-axis scaling = 1 nm).